S262: Setting up a Radio-astronomical receiver / Setting up a Radio Interferometer Lab Report

Team A5

Aarathi Parameswaran

Purbita Kole

26th Septemeber 2023

Bonn-Cologne Graduate School of Physics and Astronomy

University of Bonn

Advanced Lab Course

Winter Semester 2023/2024

Contents

1 Introduction **1**

2 Setting up a radio astronomical receiver **2**

2.1 Theoretical Background . . . 2

2.1.1 Noise Temperature . . . 2

2.1.2 Sensitivity of receivers . . . 3

2.1.3 Atmospheric attenuation . . . 3

2.2 Characteristics of Individual Receiver Components . . . 3

2.2.1 Amplifier Characteristics . . . 3

2.2.2 Filter parameters . . . 6

2.2.3 Mixer . . . 10

2.3 Measurements with a Complete Super Heterodyne Receiver . . . 11

2.3.1 Hot-cold Calibration . . . 12

2.3.2 Measurements with a Noise Diode . . . 15

2.4 Radio Spectroscopy . . . 16

2.4.1 Radio Spectrum Analysis . . . 17

2.4.2 Reception of radio FM signals . . . 20

3 Setting up a twin radio interferometer **21**

3.1 Exercises . . . 21

3.1.1 Exercise 2.1 . . . 21

3.1.2 Exercise 2.2 . . . 21

3.1.3 Exercise 2.3 . . . 21

3.1.4 Exercise 2.4 . . . 22

3.1.5 Exercise 2.5 . . . 22

3.1.6 Exercise 2.6 . . . 23

3.1.7 Exercise 2.7 . . . 23

3.1.8 Exercise 2.8 . . . 24

3.1.9 Exercise 2.9 . . . 25

3.2 Observation and analysis . . . 25

3.2.1 Experimental Setup . . . 25

3.2.2 Still Scan . . . 26

3.2.3 Declination Scan 27
3.2.4 Determination of Diameter of Sun 31

4 Conclusion **32**

1 Introduction

The aim of this experiment is to perform radio interferometry to detect radio signals from the sun. The experiment is divided into two main tasks: (1) Setting up a radio radio-astronomical receiver and (2) Setting up a twin radio interferometer and taking measurements of radio signal from the sun [1]

The first part focuses on building a superheterodyne receiver to detect radio signals and characterise various components of the receiver. The second part utilises such a receiver system to set up a twin interferometry feed and detect radio signals from the sun. The measurements are then used to reconstruct an actual radio image of the Sun projected on the equatorial coordinates.

2 Setting up a radio astronomical receiver

To perform radio interferometry we need to construct a radio signal receiver and test different components of the receivers. Also, the receiver should be able to take measurements in the radio frequency range we desire to make observations of.

2.1 Theoretical Background

The radio receiver is composed of two parts the feed/receiver and the detector part i.e the backend. Here we construct the receiver part. The main aim is to down-convert the signals to an intermediate frequency, this is achieved by a superheterodyne detector. The components of a receiver are as seen in Fig(1).

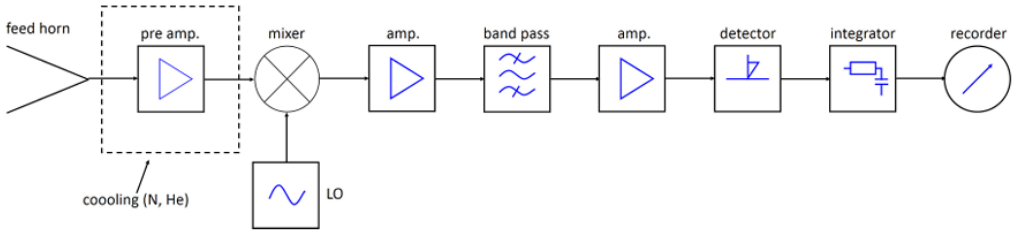

Figure 1: Block Diagram of components of a superheterodyne receiver[1]

The received radio signals are down-converted to an intermediate frequency signal using the signal from a local oscillator. The intermediate frequency is more efficient for detection by the backend. As radio signals are mostly weak pulses it needs huge amplification. Also as the detectable radio frequency is quite wide, we need to use a frequency filter to get only the desired radio signal. This also leads to more sensitive detection of radio signals.[1, 2]

2.1.1 Noise Temperature

Each of the active components of the receiver contributes to a noise in the signal due to the intrinsic thermal radiations. So noise temperature can be defined as the ideal temperature if the receiver has no input signal. The total noise temperature of the receiver is contributed by its individual components.[1]

$$T_{rec} = T_1 + \sum_{i=2} \frac{T_i}{\prod_{k=1}^{i-1} G_k} \tag{1}$$

where G is the gain of the individual components.

2.1.2 Sensitivity of receivers

The radiometer equation in Equation(2) is used to measure the quality of a radio astronomical observation.

$$\Delta T = \frac{T_{sys}}{\sqrt{\Delta t \Delta \nu}} \tag{2}$$

where ΔT is the uncertainty in the determination of source brightness temperature, T_{sys} is the system temperature as defined in $\Delta\nu$ is the bandwidth and Δt is the integration time. The product of the integration time and the bandwidth is proportional to the amount of energy received, and the higher the integration time, the more the number of received photons. The Signal-to-Noise (SNR) of the signal is then just determined by the ratio of antenna temperature and uncertainty in the temperature(ΔT).[2]

2.1.3 Atmospheric attenuation

The total temperature of the antenna is affected by the background temperature (from various sources like cosmic signals, BB radiation of ground etc) and also the temperature of the atmosphere. The atmospheric temperature depends on the total column of water traversed by the signal. Also, atmospheric gases which emit radiation also lead to absorption of the signals. So atmospheric radiation decreases the SNR of radio signals. The atmospheric attenuation can be given by the radiative transport equation given by[2]-

$$T_A = T_{sys} - T_{rec} = e^{-\tau} T_B + (1 - e^{-\tau}) T_{atm} \tag{3}$$

where T_A is the antenna temperature, T_{sys} is the temperature of the system /source temperature,τ is the optical depth (this is also expressed as the attenuation $L = e^{\tau}$),T_B is the background temperature and T_{atm} is the atmospheric temperature.

2.2 Characteristics of Individual Receiver Components

2.2.1 Amplifier Characteristics

Amplifiers are used to 'amplify' input signals to output signals having higher power. Amplifiers are an important part of radio astronomical setup due to low-power radio signals. The amplifier characteristics were analysed by looking at the plot of input and output power. The characteristics to be measured of the amplifier are -

- **Gain** measured from the average ratio of input and output power

- **Saturation Power** The power after which the signals show no characteristic increase.

To measure the characteristics the amplifiers were arranged according to the circuit in Fig(2). The power meter values are plotted against input power as seen in Figs(**??**). As the amplifier is expected to show a linear characteristics, the graph was fitted with a linear fit($y = mx+b$)for the non-saturating region. The fit was done using `scipy.optimize.curve fit` which uses the least-squares method for fitting[1]. In the non-linear part of the graph, the mean saturating power was calculated using `numpy.mean()` The parameters from the fits obtained are shown in Table(1) [2]

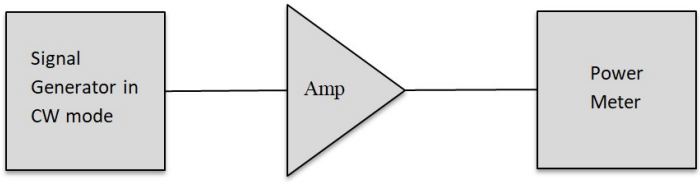

Figure 2: The circuit setup to measure the characteristics of the three different amplifiers

Name	**Function**	**Bandwidth**	**Central** ν	**Gain**
HF V1	HF Pre-amplifier	2-3 GHz	2.3 GHz	0.87449 ± 0.00026
HF V3	HF -amplifier	2-4 GHz	2.3 GHz	0.91502 ± 0.00012
ZF V1	IF Amplifier	10-500 Mhz	150 Mhz	0.95675 ± 0.00006

Table 1: Parameters of amplifiers

[1] All fits from here are calculated using the same method

[2] **Ex 1.1**

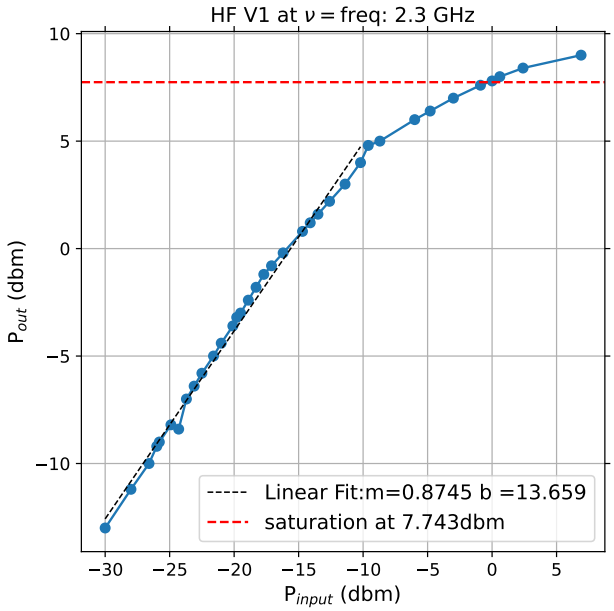

Figure 3: Amplifier characteristics of High Frequency V1 amplifier

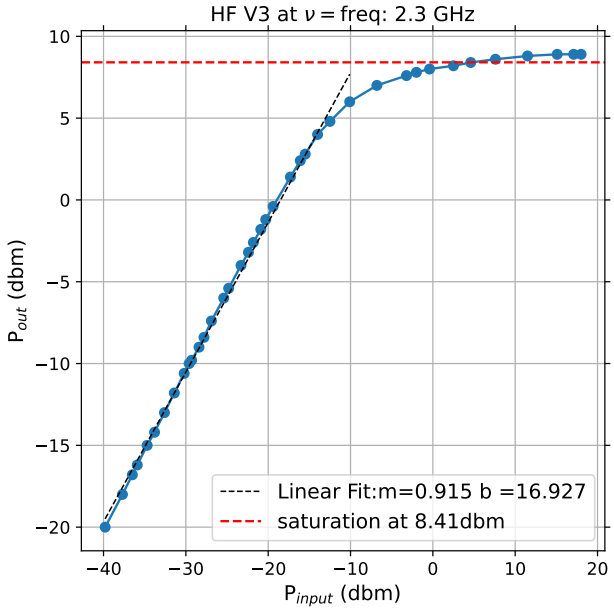

Figure 4: Amplifier characteristics of High Frequency V3 amplifier

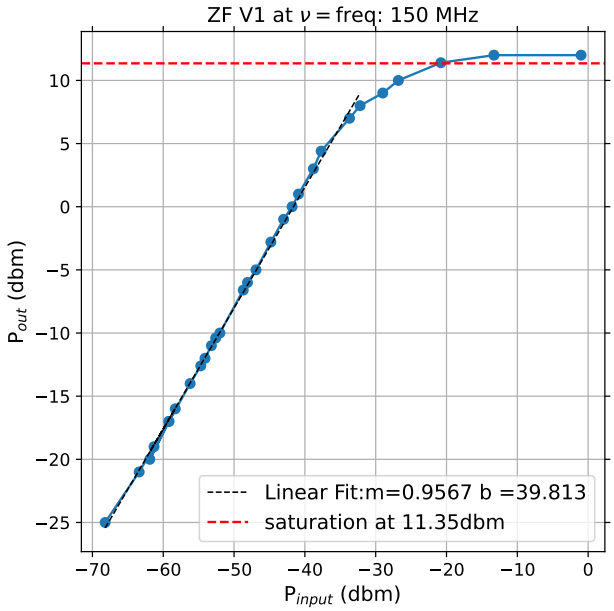

Figure 5: Amplifier characteristics of Intermediate frequency ZF V1 amplifier

2.2.2 Filter parameters

Filters are used to select only a particular frequency range of the spectrum or a band-pass. The parameters of filters of importance are

- **3 dBm gain/loss** 3 dBm gain/loss of the signal is an important parameter as it determines the point where the signal is double/half of the original signal(or maximum of the signal) [3]

- **Bandwidth** It is the range of the frequency within which the peak of the radio signal lies

- **Insertion Loss** It is the ratio of the value of the unfiltered signal and the filtered signal

$$\text{Insertion Loss} = 20log_{10}(\frac{|P_{in}|}{|P_{out}|}|) = 2(|P_{in} - P_{out}|) \tag{4}$$

  It gives an estimate of how much of the signal is filtered.[4]

- **Side attenuation** It is the attenuation of the sidebands (the frequency bands whose output is filtered) compared to the maximum output power of the filter.[5]

- **Adjacent Band Rejection** It is the frequency range for signals within 60 dBm and 3 dBm below the maximum output of the filter. [5]

For measurement of these parameters, the two filters are arranged as shown in Fig(6). For the calculation of Adjacent Band rejection, the lowest frequency is taken instead of -60 dBm as no data lower than -30 dBm was recorded for both filters.[3]

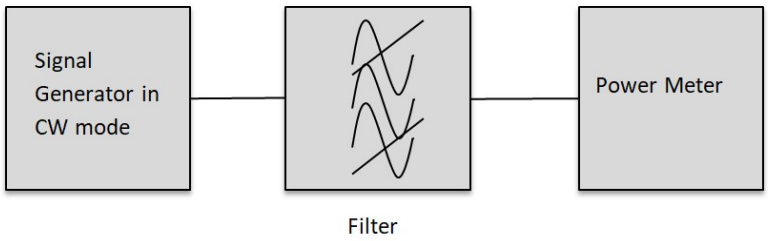

Figure 6: The circuit setup to measure the filter signal of the two different filters

Name	**Bandwidth**	**Central ν**	**Filter Output Power (dBm)**	**Adjacent Band Rejection**	**Side Attenuation**	**Insertion Loss (dBm)**
ZF F1	55 MHz	150 MHz	2.48 ± 0.17	25 MHz	0.32 ± 0.07	5.05 ± 0.34
HF F1	0.082 GHz	2.3 GHz	-5.5 ± 1.1	0.1536 GHz	0.18 ± 0.04	21.0 ± 2.2

Table 2: Parameters of Filters calculated from the filter signal in Figs(7,8)

in Fig(7), a plateau-like structure with steep slopes is seen as expected. It implies a quick transition to the desired bandwidth and for a number of values in the bandwidth the output signal is maximum. In Fig(8), the Gaussian curve signifies the filter is not sensitive and only gives maximum output for a few values in the bandwidth. From the figures we can see filter needs to be operated at the plateau region, to achieve maximum power output in the bandwidth.

[3] **Ex 1.2.**

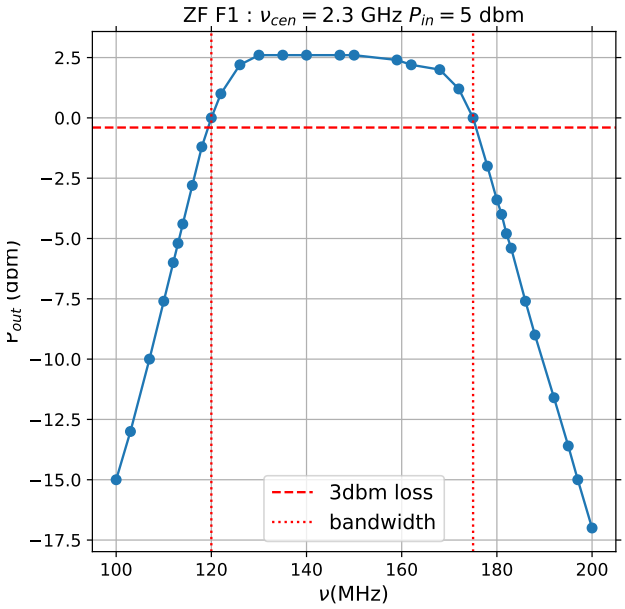

Figure 7: Signal of the filter ZF F1 working at an input of 5 dBm.

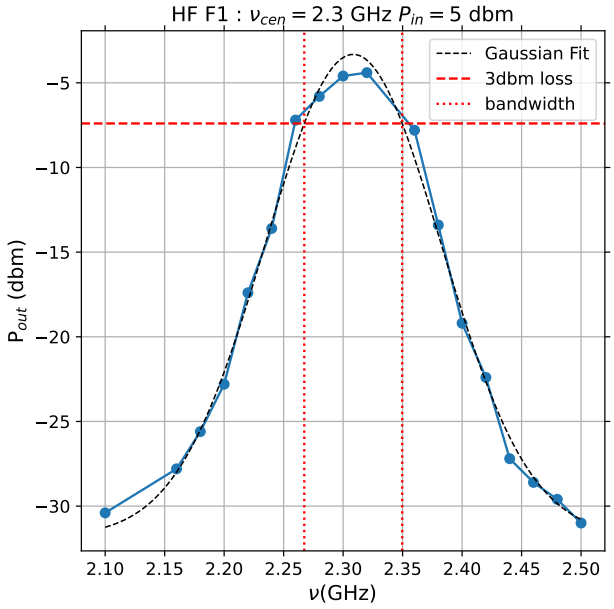

Figure 8: Signal of the filter HF F1 working at an input of 5 dBm.

Now instead of the power meter, the filter is attached to the oscilloscope. So we see the

entire output frequency spectrum of the filter. [4]

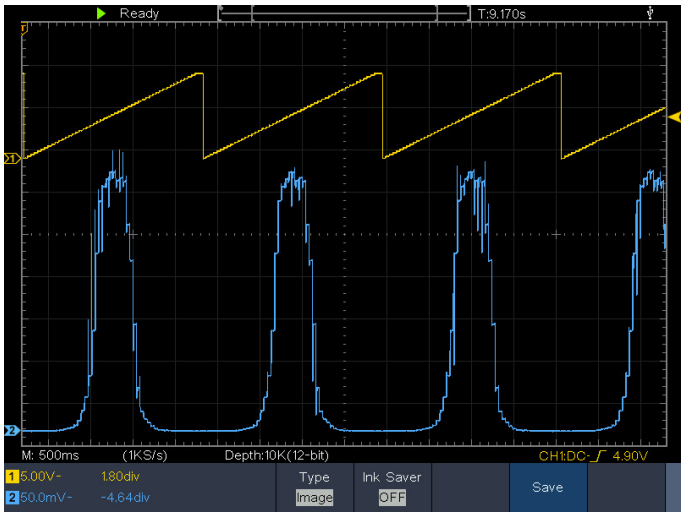

Figure 9: Real-time oscilloscope signal of the filter HF F1

As seen in Fig(10), on varying the central frequency the Gaussian curve is shifted.

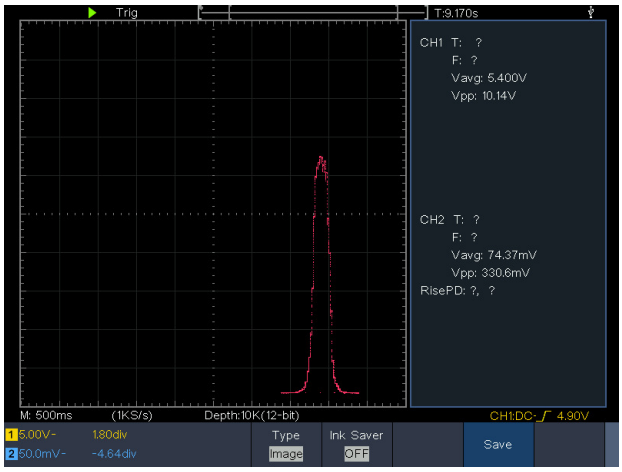

Figure 10: Shift of the filter signal as seen in oscilloscope window, on shifting the central frequency of the filter.

[4] **Ex 1.3**

2.2.3 Mixer

The mixer is the part of the receiver which is responsible for the heterodyne detection and the down-conversion of the radio signal. The mixer is generally connected to a local oscillator on one end and the other end receives the radio signal from the filter. The important characteristic of a mixer is Conversion Loss i.e. the loss in power of signal after down-conversion. It is calculated using [6]

$$L_c = 10log\frac{\text{RF input power}}{\text{IF output power}} = \frac{10\text{RF input power(in dBm)}}{\text{IF output power(in dBm)}} \tag{5}$$

The mixer was arranged according to the circuit in Fig(11) In Fig(12)).Here the signal generator at 2.45 GHz behaved as a local oscillator and the other signal generator at 2.3 GHz acted as a radio signal. The values from the power meter were plotted vs the RF input which was varied using the signal generator. A linear fit($y = mx + b$) was applied to the graph of RF input vs the power output of the mixer. the conversion loss was found to be $\mathbf{12.278 \pm 0.014\ dBm}$. General typical values of such ranges from 3 dBm to 10 dBm[7] [5]

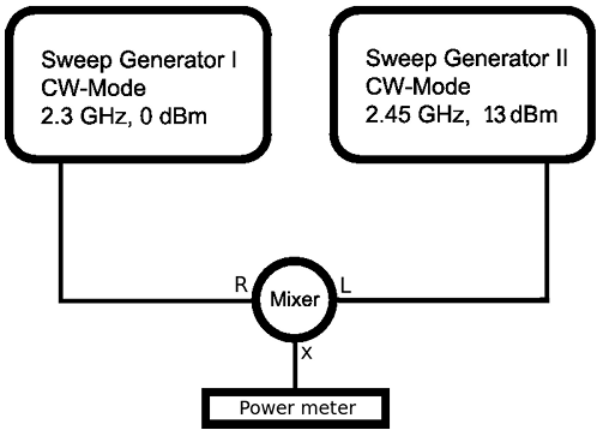

Figure 11: Circuit for measuring the power output of a mixer for detecting radio signals[1]

[5] **Ex1.4**

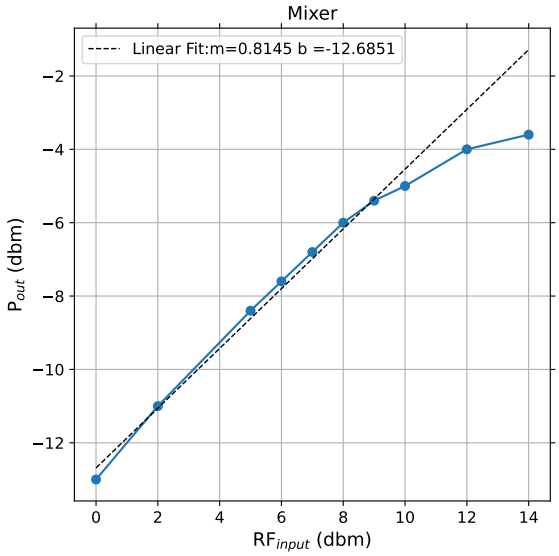

Figure 12: Power output of the mixer on varying the input radio signal

2.3 Measurements with a Complete Super Heterodyne Receiver

For this experiment, a complete superheterodyne setup was already present The construction of the receiver is as seen in Fig(13).

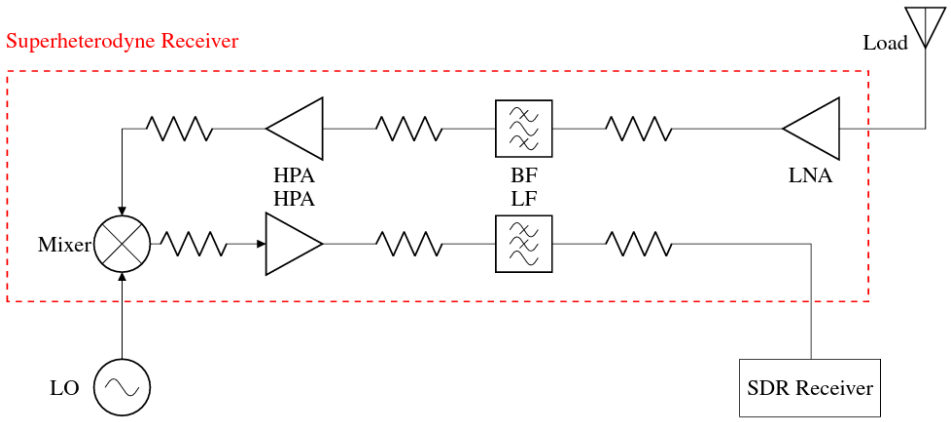

Figure 13: Complete circuit of the superheterodyne receiver. Here the load acts as the radio signal and the SDR receiver is used as an output receiver. SDR receiver can also be connected to the computer [1].

This setup can be directly used to measure radio signals by connecting a feed to it.

Here it is used to measure noise temperature of different electronic devices and man-made radio signals used for analysis. The SDR receiver is connected to the computer unit. The Gqrx software helps in visualising the output power signal. Two predefined Python codes were available. One was used to measure the power while the other was used to measure the spectrum of the signal.

2.3.1 Hot-cold Calibration

Calibration of such a receiver requires, calculating the trend in noise temperature. This is done by measuring the power of a 50Ω resistor at room temperature and at the temperature of liquid nitrogen(77±0.5K). Such a cold temperature is quite helpful as it considerably reduces noise. After calibration, receiver temperature could be estimated using equation[1]-

$$T_{rec} = P_{cold}\frac{T_{hot} - T_{cold}}{P_{hot} - P_{cold}} - T_{cold} \tag{6}$$

To perform the hot-cold calibration, the superheterodyne receiver was set up as shown in Fig(14). The room temperature was measured to be $295K$ and a reading error of $5K$ was considered too. From Gqrx software, the power readings were initiated. After 15 s the resistor was dipped in liquid nitrogen and readings were taken till bubbles topped forming on the surface of the liquid nitrogen[6]

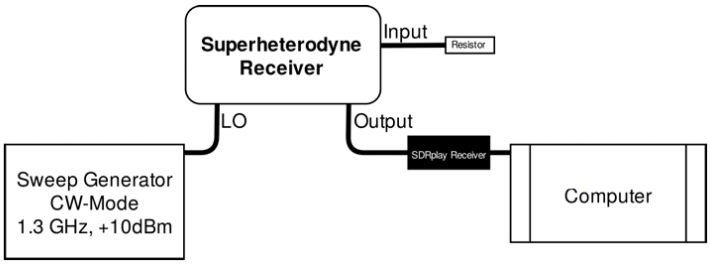

Figure 14: Setup for measuring the power of an active electronic device or signal attached as a load to the superheterodyne receiver[1]

The power readings in dBm were obtained from the Python codes and were plotted against the time taken for measurement as seen in Fig(15). From the graph, the mean value of power for room temperature and cold temperature were calculated and their standard

[6]**Ex 1.5**

errors were also derived. The power from the program is expressed in dBm, it can be converted to mW using Eq(7).From Fig(15), the parameters calculated are

$$P(mW) = 10^{\frac{P(dbm)}{10}} \tag{7}$$

- Power at room temperature i.e
  $\mathbf{P_{room}} = \mathbf{-3.739 \pm 0.03218}$ dBm $= \mathbf{0.423 \pm 0.0031}$ mW
- Power at temperature of liquid nitrogen i.e
  $\mathbf{P_{cold}} = \mathbf{-5.0108 \pm 0.03367}$dBm $= \mathbf{0.3154 \pm 0.00244}$mW

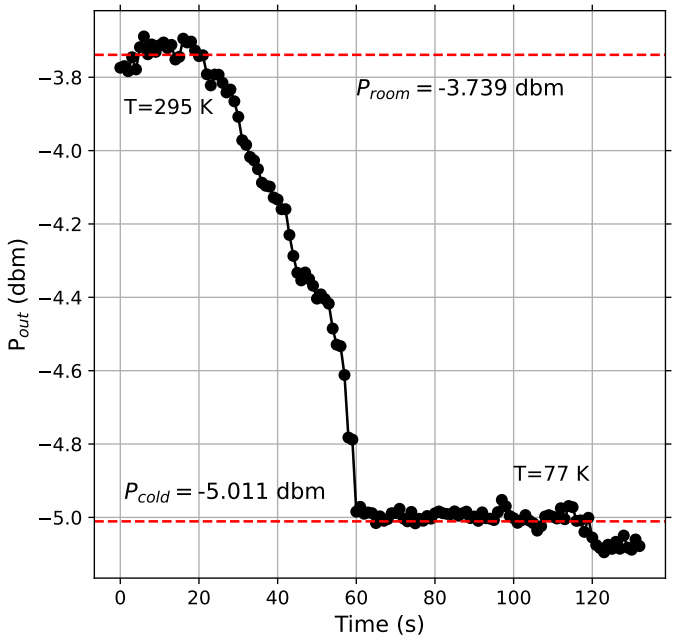

Figure 15: Hot-cold Calibration Curve

In order to calibrate other values, we need the values of slope and intercept of the graph of power output expressed in mW and temperature expressed in K. As seen in Fig(16), the values of power at room temperature and at the temperature of liquid nitrogen were plotted. The data was also extrapolated, to get the temperature where the output power is negligible i.e. the noise temperature. A linear fit (using the same method as before) was then applied to the fit

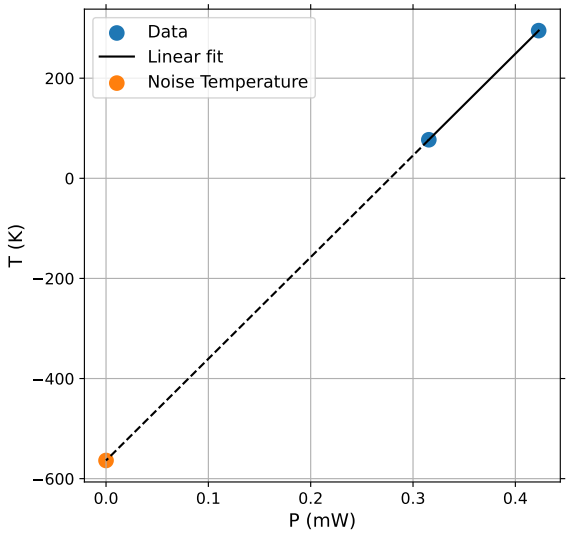

Figure 16: Linear Fit on the hot-cold calibration points and the extrapolated noise temperature value

From the graph , **slope** was found to be $\mathbf{2031.043 \pm 1.53 K/dBm}$ and the intercept was found to be $\mathbf{-563.675 \pm 1.089\ K}$. The receiver temperature i.e. the noise temperature of the receiver was also estimated using the formulae(Eq(6) using values of power and temperature calculated before. The Gaussian errors for the formulae were calculated in PYTHON using the UNCERTAINITIES package.[7] The receiver temperature was thus found to be

- T_{rece}(graphically)=$\mathbf{-563.675 \pm 1.089\ K}$
- T_{rece}(using formulae)=$\mathbf{-564 \pm 3.4\ K}$

So the two values agree well within their error limit. This calibration can be further used to determine the noise temperature of various receivers.

[7]In the UNCERTAINITIES package[8], one can declare any value along with their error value as an `ufloat(), uarray()` object. Any further calculation with those values will calculate the corresponding Gaussian error. From here onward for calculating Gaussian error this method is used.

2.3.2 Measurements with a Noise Diode

Now, the noise temperature of a noise diode is to be determined, where the resistor in Fig(14) is now replaced by a noise diode. Then using the same steps as before the power measurements of the noise diode were taken for an integration time of 10s.[8]
The average output power of the noise diode was found to be $\mathbf{-1.709 \pm 0.016\ dBm}$ or $\mathbf{0.6746 \pm 0.0025\ mW}$. Using the hot-cold calibration values from before, the noise temperature of the noise diode was calculated to be $\mathbf{807 \pm 5\ K}$.

Simulating Atmospheric Attenuation

For building a working superheterodyne receiver, the attenuation of the atmosphere must be simulated and the working of the receiver at those frequencies should be checked. In this experiment, we have done so by changing the attenuation of the noise diode and analysing the change in power with the change of attenuation level. The graph of the receiver temperature and the variable attenuation should exhibit an exponential decrease as per the radiative transport Eq(3).[9]
For this experiment, a variable attenuator was attached between the noise diode and receiver. Using the same steps as before, power measurements were taken for attenuation values between 0 dBm to 30 dBm. All measurements were obtained for an integration time of 10s. The average power values for each attenuation and their corresponding errors were calculated. Using the hot-cold calibration the variable receiver temperature was derived. The graph of the receiver temperature and attenuation (converted to mW scale) was plotted (as seen in Fig(17) and the equation for radiation transport (Eq(3)) was fitted. As seen in Fig(17) the receiver temperature exponentially decreases with an increase in attenuation. This simulates the attenuation of the atmosphere as the optical thickness of the atmosphere increases with respect to radio signals. From the fit the **background temperature**($\mathbf{T_B}$) was found to be $\mathbf{1143.88 \pm 10.55K}$ and the **atmospheric temperature**($\mathbf{T_{atm}}$) was found to be $\mathbf{635.45K \pm 20.55K}$.

[8] **Ex1.6**
[9] **Ex 1.7**

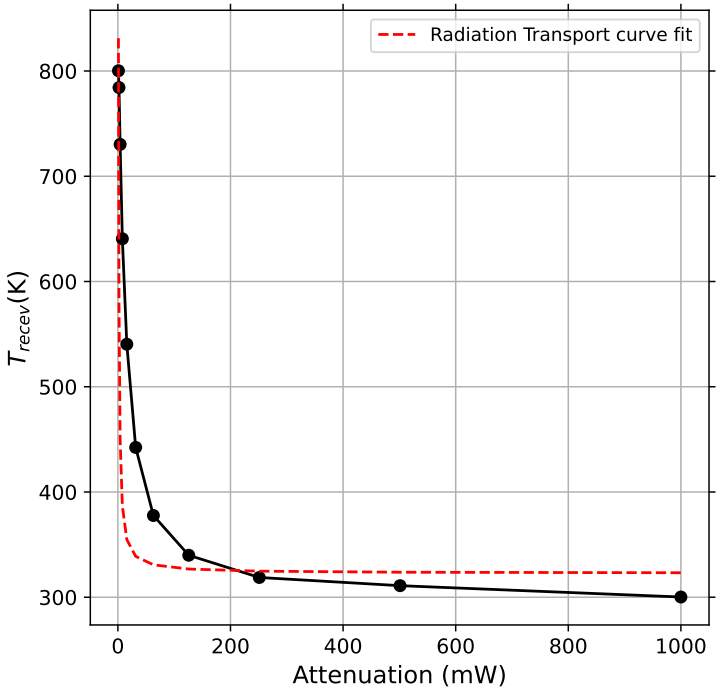

Figure 17: Plot of exponential decrease for receiver temperature with increase in attenuation

2.4 Radio Spectroscopy

To mimic the radio FM signals and to analyse the characteristics of the radio spectrum, a spectrum analyser was attached to the receiver. The local oscillator was modified and the signal generator was used to generate the artefact FM signal and the output was displayed on the spectrum analyser. The signal generator was used to produce a signal 1.35GHz at -10 dBm. While the LO was set in Continuous Wave mode at 1.2GHz at an output power of 10 dBm. The spectrum analyser helps in analysing the bandpass of the signal. From the given settings we see that the intermediate frequency to be produced is

$$\nu_{IF} = |\nu_{LO} - \nu sig| = |1.2 - 1.35|\text{GHz} = 0.15 \text{ GHz or } 150\text{MHz}$$

As we can see in Fig(18a), in the display of the spectrum analyser, the peak of the signal is at 150 MHz. This implies that the superheterodyne output is well within the predicted

output. In Fig(18b), as we change the signal artefact, the peak shifts and also slowly moves outside the bandpass of the superheterodyne receiver.[10]

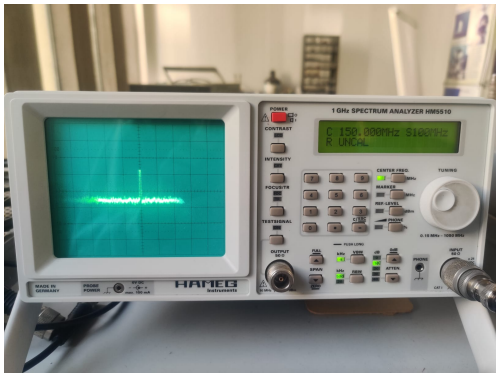

(a) 150 MHz

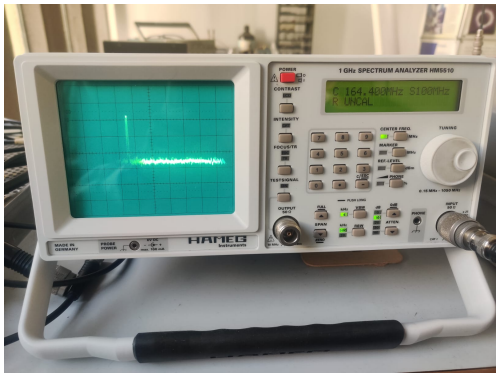

(b) 164 MHz

Figure 18: Display of the spectrum analyser showing the radio bandpass signal for different input frequency

2.4.1 Radio Spectrum Analysis

Now we want to analyse the spectrum of this radio signal and also the sensitivity of the receiver based on the integration time. So we switch back the setup to the configuration in Fig(14). The measurements were taken for different integration times from 10s to 180s. Both the information of the power and the spectrum of the measurements were generated using the Gqrx software and the pre-defined python codes[11].

The average power for each integration time was obtained and converted to receiver temperature using the hot-cold calibration. In Fig(19), a general trend of a slight increase in receiver temperature can be observed with an increase in integration time. This is due to an increase in the Signal to noise ratio with an increase in integration time. The average receiver temperature over all the integration time was calculated to be $\mathbf{1748 \pm 14K}$.

From the radiometer equation (Eq(2)) we see that the noise in the output power should decrease with an increase in integration time in a quadratic trend. So the rms noise in temperature for different integration times was plotted taking the average receiver temperature as the system temperature using the radiometer equation.The $\Delta\nu$ value in the Eq(2) was taken to be 3 ± 0.5MHz. The values obtained were plotted as seen in Fig(20)

[10] **Ex 1.8**

[11] **Exercise 1.9**

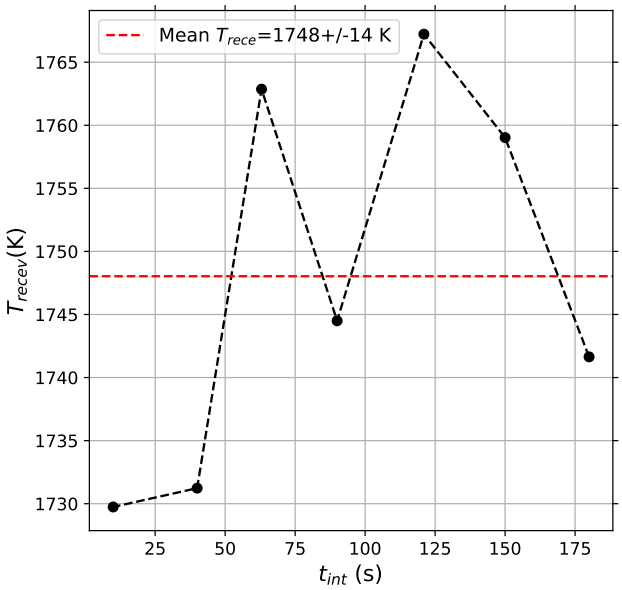

Figure 19: Plot of receiver temperature for different integration time

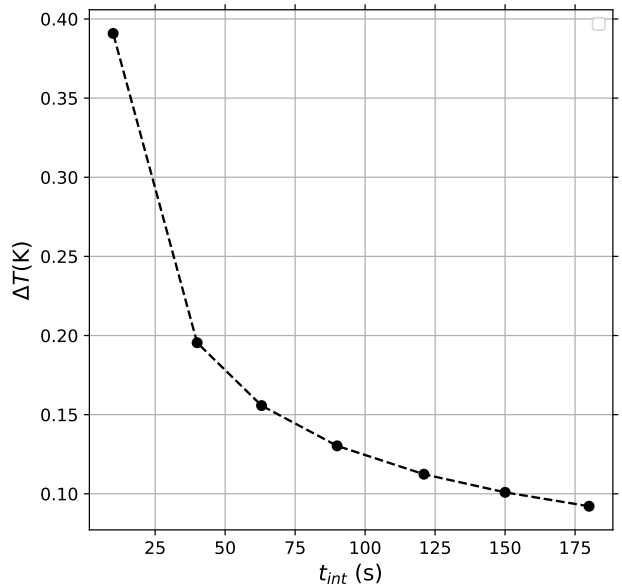

Figure 20: RMS noise of the signal plotted against the integration time

The spectrum of the radio signal for each measurement value was also obtained. The

intensity value against the frequency was also plotted as seen in Figs(21a,21b). As expected the radio signal peak is positioned at **150MHz**. For each integration time, the max intensity was measured. the line flux of the entire spectrum was also calculated using the PYTHON function `np.trapz()`, which performs integration of the Intensity values using the trapezoidal method. The values are given in Table(3).

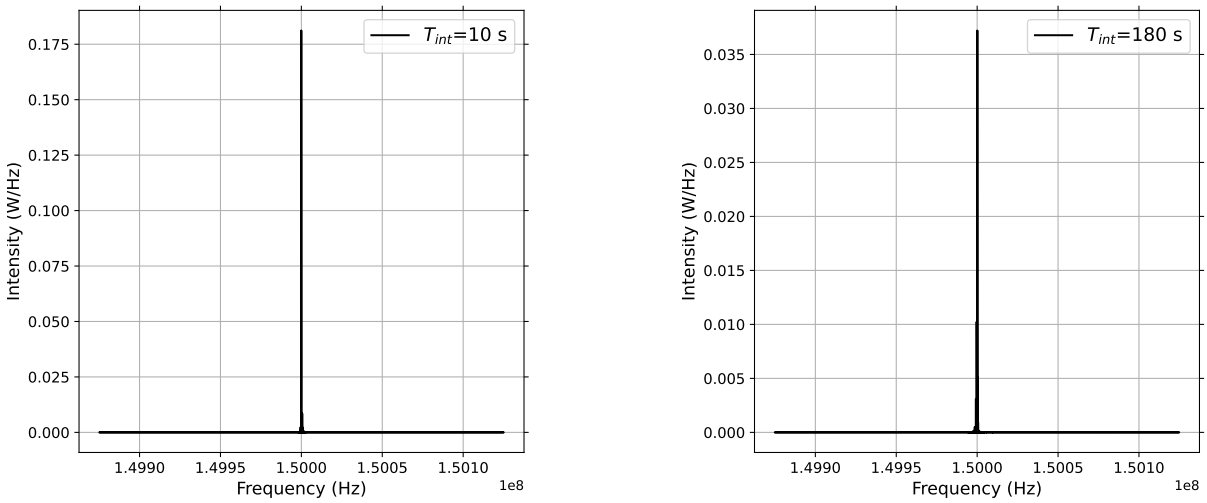

(a) Radio spectrum for integration time of 10s

(b) Radio spectrum for integration time of 180s

Figure 21: Radio Spectrum for different integration time

Assuming, the cloud in thermal equilibrium as a blackbody. For radio emission, we can approximate Planck's law to express the brightness temperature of the thermal gas cloud as -[2]

$$T_B = \frac{B(\nu)_{max} c^2}{2 k_B \nu^2} \tag{8}$$

where T_B is the brightness temperature, $B(\nu)$ is the spectral flux density which can here be taken from the maximum intensity of the spectrum, ν is the frequency of the spectrum. Here the frequency is $\mathbf{1.5 \times 10^8}$ **Hz** and the other terms are the speed of light and Boltzmann constant. The calculated values of the brightness temperature are given in Table(3).

Integration Time (s)	Line Flux (W)	Maximum Intensity (W/Hz)	Brightness Temperature (K)
180	0.54528	0.03722	5.38421241e+21
150	0.57072	0.0366	5.29448074e+21
121	0.58754	0.02927	4.23428951e+21
90	0.54944	0.01863	2.69468773e+21
63	0.5911	0.00808	1.16815170e+21
40	0.52973	0.04348	6.28999024e+21
10	0.53135	0.1812	2.62126768e+22

Table 3: Parameters of radio spectrum

2.4.2 Reception of radio FM signals

To calculate the ideal antenna length for transmission of radio signal at 100 MHz, we need to first consider the wavelength of the signal

$$\lambda = \frac{c}{\nu} = \frac{3 \times 10^8}{100 \times 10^6} m = 3m$$

Now the construction of the antenna will determine the length of the antenna. Generally for such radio FM signal, a dipole antenna is constructed. The dipole antenna works efficiently at $\lambda/2$or $\lambda/4$ configuration (due to resonances of the radio waves). So the antennas, here should ideally be at $\lambda/2 = 1.5$m or $\lambda/4 = 0.75$m in length.[9][12]

Broadcasting Radio signals:

Using the signal generator, an FM radio signal was also broadcast. This was done by tuning the signal generator to a free frequency (100 MHz was chosen). The radio player in the room was also tuned to this frequency. The signal generator has an antenna attached to its output, and an input available to plug in an audio device. By setting the signal generator to the 'FM modulation' mode and changing the settings appropriately, the sound of the frequency set at the signal generator could be heard playing from the radio receiver. Changing the 'FM dev frequency' changed the volume of this sound, and changing the 'FM rate' changed the pitch of the sound (the frequency). On attaching an audio device (a mobile phone) and changing the source settings on the signal generator, the music playing on the phone could be heard over the radio.

[12] **Exercise 1.10**

3 Setting up a twin radio interferometer

3.1 Exercises

3.1.1 Exercise 2.1

Which property of the telescope can affect angular resolution and image quality?

The angular resolution θ of a radio telescope is given by:

$$\theta = 1.22\frac{\lambda}{D} \tag{9}$$

where λ is the wavelength, and D is the diameter of the dish or the baseline in an interferometer. From the equation, it can be seen that there is an inverse relationship between the diameter of the dish and the angular resolution.

3.1.2 Exercise 2.2

What is the difference between the wavelengths of operation at radio telescopes with small and big parabolic surfaces?

From equation(9), we can see that for a given angular resolution, a larger parabolic surface will have to operate at larger wavelengths and a smaller parabolic surface will have to operate at a smaller wavelength.

3.1.3 Exercise 2.3

How can you prove the equality of the altitude of the north celestial pole and the latitude of the observer?

In figure(22), angle A is the altitude of the north celestial pole and $B + D + A = 90°$ since that is the angle between the horizon and the zenith. $B + D = C$ because they are opposite angles. C is a part of a right-angled triangle with the latitude so $C + L = 90°$. Hence, $C + A = 90°$ and $C + L = 90°$, therefore, $A = L$.

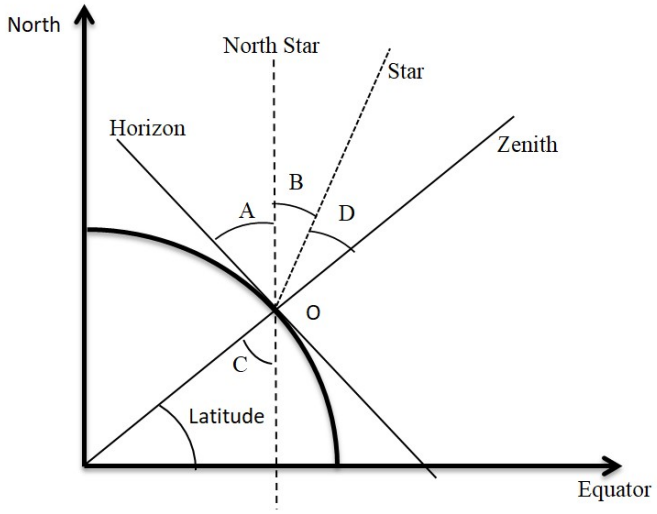

Figure 22: Equatorial Coordinate System diagram

3.1.4 Exercise 2.4

How many full moons can be laid side-by-side within Polaris' circular path about the north celestial pole?

Given that the angular diameter of the moon is about $30'$, and polaris is $1°$ away from the north celestial pole [1], the diameter of the circular path of polaris is $2°$. Knowing that $1° = 60'$:

$$Number of moons = \frac{2 \times 60'}{30'} = 4 \tag{10}$$

4 full moons can be laid side-by-side within Polaris' circular path about the north celestial pole.

3.1.5 Exercise 2.5

Solar atmosphere has three main layers: the photosphere, the chromosphere and the corona. What kind of emission does each layer emit? Which layer(s) does(do) emit in radio wavelengths?

The photosphere is the deepest layer of the atmosphere of the sun. It is characterised by the presence of spicules. It emits mainly at optical wavelengths, in the visible spectrum. The chromosphere is the layer above the photosphere which emits in UV and radio wavelengths. The height of the chromosphere is roughly the same as that of the photosphere.

The corona is the outermost layer of the sun with an indefinite extent that produces solar winds and flares. It emits in radio, UV and X-ray wavelengths [10, 11].

3.1.6 Exercise 2.6

What is the origin of the radio emission of the corona?

The radio emission of the corona comes from the processes of thermal bremsstrahlung (where electrons are deflected by the electric fields of ions), gyromagnetic emission (where electrons are accelerated by the external magnetic fields) and other processes like synchrotron radiation and plasma emission [12].

3.1.7 Exercise 2.7

Plot the flux density vs. frequency for three different sources (e.g. 1000, 4000, 8000) and place the solar emission profile on it. Does the Sun have a perfect black body radiation?

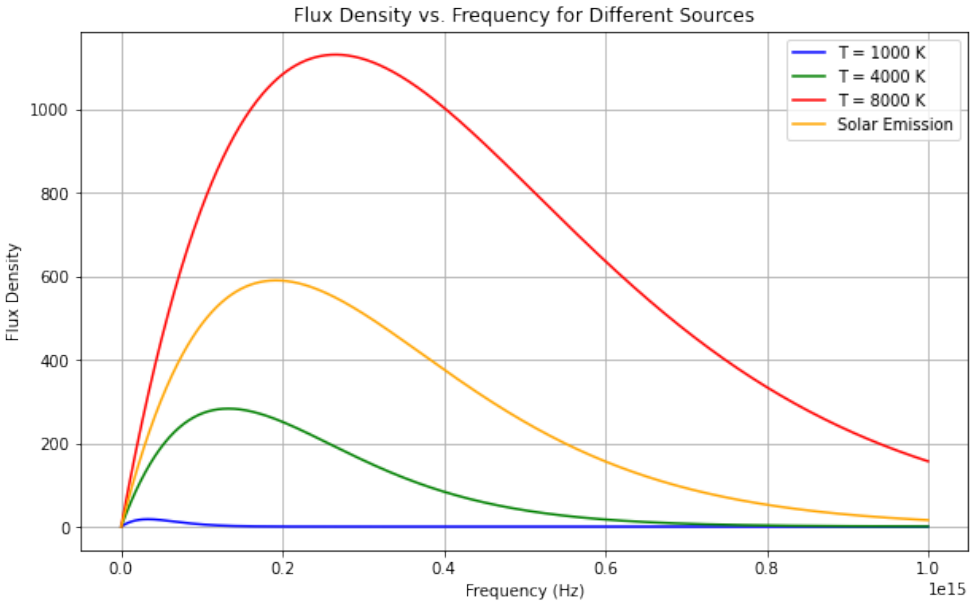

Figure 23: Flux density vs frequency

Figure(23) shows the flux density vs. frequency for three different sources and the solar emission profile. The sun does not have perfect black-body radiation as it has emission

across a broad range of wavelengths and Planck's law is a useful approximation for this [13].

3.1.8 Exercise 2.8

What is the difference between the radio emission of the active Sun and the quiet Sun? Locate both in the plot.

The sun has a solar activity cycle that is seen by the changing number and location of sunspots visible on the surface of the sun, the level of solar radiation, the luminosity, and solar flares. This magnetic cycle has an average period of 11 years. The quiet sun is the phase of the cycle with lower solar activity, typically seen by a reduced number of sunspots. The active sun is the phase with higher solar activity [14].

Solar radiation spectrum covers all wavelengths from radio to optical. At optical wavelengths, the sun can be treated as a blackbody with a constant temperature of 6000K. But in the radio frequency band, the radiation flux changes over the solar cycle, and the radiance for the active and quiet sun is significantly different. The active sun has a much larger flux density than the quiet sun [15]. These effects can be seen in figure(24).

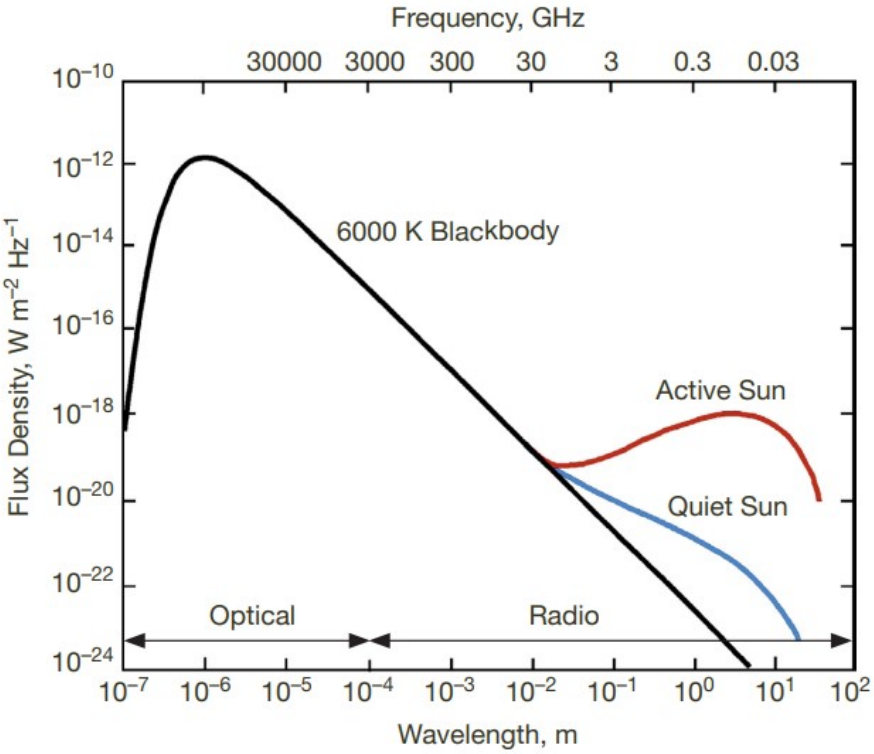

Figure 24: Difference in the radiance of active and quiet sun at radio wavelengths [15]

3.1.9 Exercise 2.9

In which case can we see the Sun bigger in size? Observing the photosphere or the corona?

The sun appears to be bigger when we observe the corona because the corona mainly emits radio wavelengths and it is the outermost layer of the sun's atmosphere with an indefinite extent, i.e. it has no upper limit [16].

3.2 Observation and analysis

3.2.1 Experimental Setup

The observations for the experiment are made with a twin radio interferometer consisting of two 90 cm dish antennas on an equatorial mount. The operation is done in the X Band of frequencies in the radio region, the frequency range is approximately between $7 - 11.2GHz$ [17]. A transit observation of the sun using a still scan and declination scan

was performed to obtain the fringe pattern and then used to produce an image of the sun. The alignment was done by using the shadow of the detector on the hole in the middle of the dishes.

3.2.2 Still Scan

To perform the still scan, the detector's shadow is aligned tangentially to the hole on the dish and the observation is done without moving the antennas, the Sun passes in front of the detector due to Earth's rotation for which the data is collected [1]. A still scan schematic can be seen in figure(26).

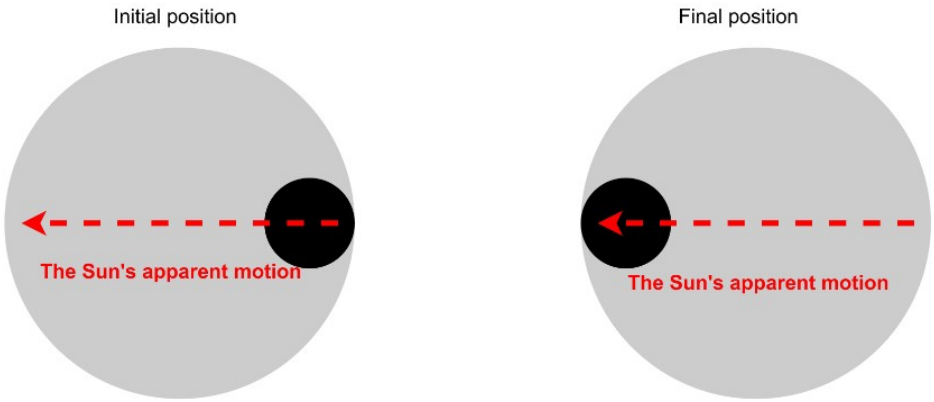

Figure 25: Schematic of the still scan [1]

The raw data obtained from both antennas can be seen in figure(26).

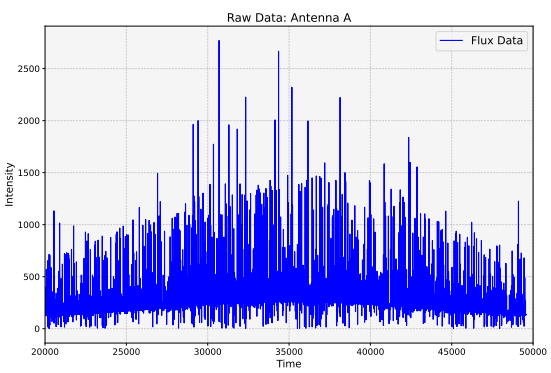

(a) Raw data for the first antenna

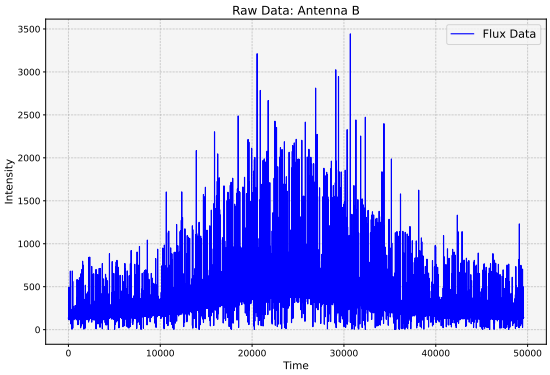

(b) Raw data for the second antenna

Figure 26: Raw data for the still scan

Given the amount of noise from various sources, noise reduction of the data is a necessary procedure in the data reduction. The data reduction is done iteratively, with a loop iterating eight times and calculating the difference between a given data point and the corresponding point shifted by two positions on either side. If this is greater than a certain threshold defined for a given quantity, that data point is removed. This is done to effectively remove outliers that deviate significantly from their neighbours.
The denoised data obtained can be seen in figure(27). After the denoising procedure, we can see the variation in the intensity as the sun moves through the beams of the telescope.

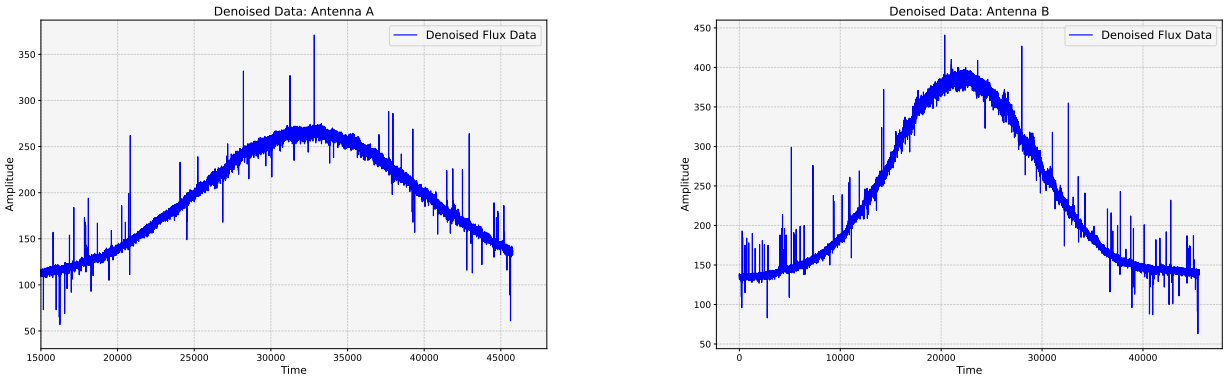

(a) Denoised data for the first antenna

(b) Denoised data for the second antenna

Figure 27: Denoised data for the still scan

3.2.3 Declination Scan

A declination scan is also performed, which uses the RA and dec. mounts of the dishes. The dishes are periodically moved up and down in the declination plane, keeping the right ascension constant and the sun's 'image' is allowed to pass in front of the dish naturally. Again, the detector shadow on the dish is used for alignment. The path of the sun can be seen in the schematic in figure(28).

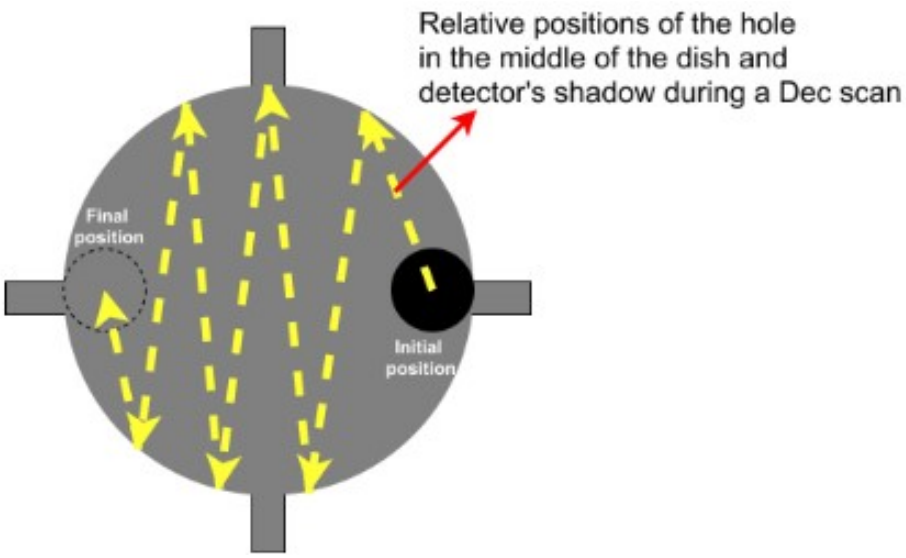

Figure 28: Schematic of the declination scan [1]

The raw data can be seen in figure(29) and the denoising procedure followed is the same as that in the still scan. The denoised data obtained is seen in figure(30).

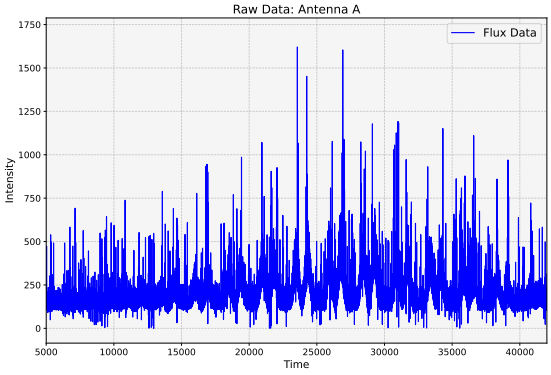

(a) Raw data for the first antenna

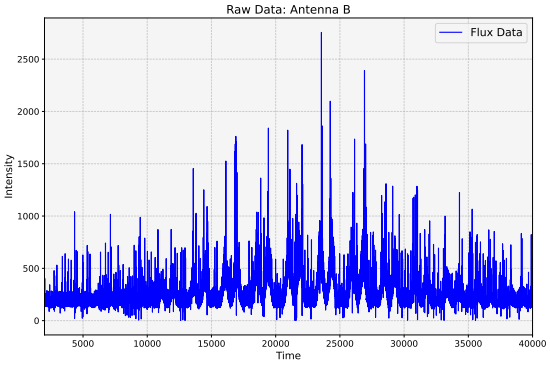

(b) Raw data for the second antenna

Figure 29: Raw data for the declination scan

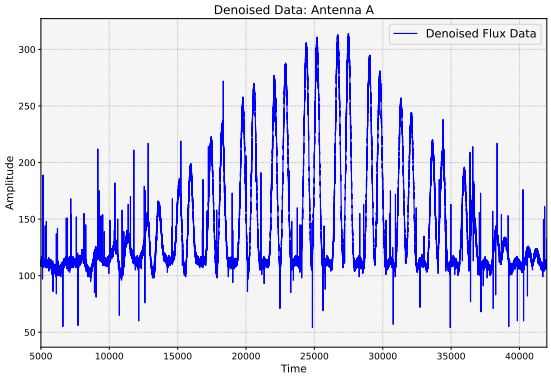

(a) Denoised data for the first antenna

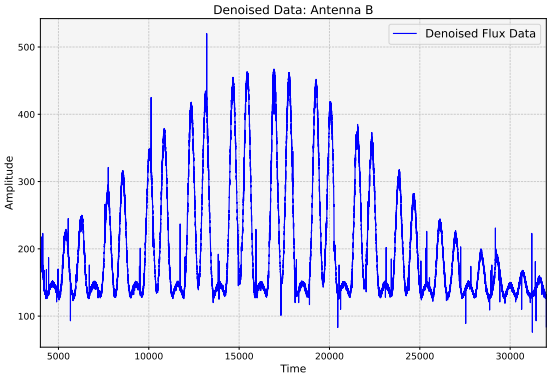

(b) Denoised data for the second antenna

Figure 30: Denoised data for the declination scan

After denoising the data for the declination scan, we create a 2D image of the sun. For each measurement in the plot for intensity vs. time, we have the RA and Dec coordinates. This is essentially the pointing of the telescope or the field of view and we can plot the right ascension vs. the declination, as seen in figure(31).

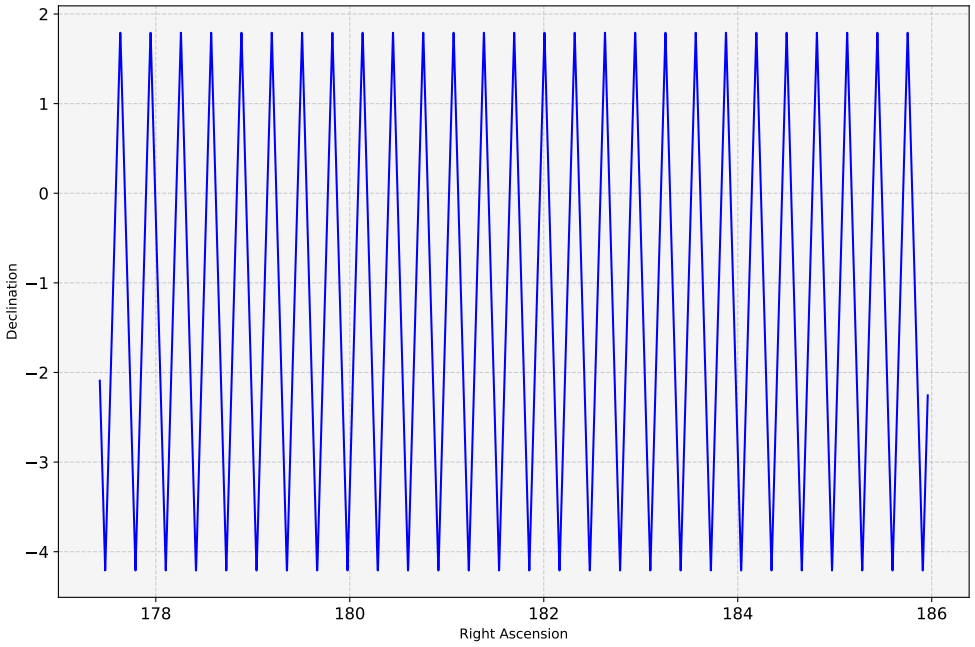

Figure 31: Right Ascension vs. Declination of the telescope in the declination scan.

The intensity along the path in figure(31) is recorded and on an empty 2D grid, we interpolate the values using the RA, dec., and intensity to obtain the 2D images of the sun

for each of the antennas, as seen in figure(32) and for both as the twin interferometer, as seen in figure(33). The interferometric image combines the data from both antennas.

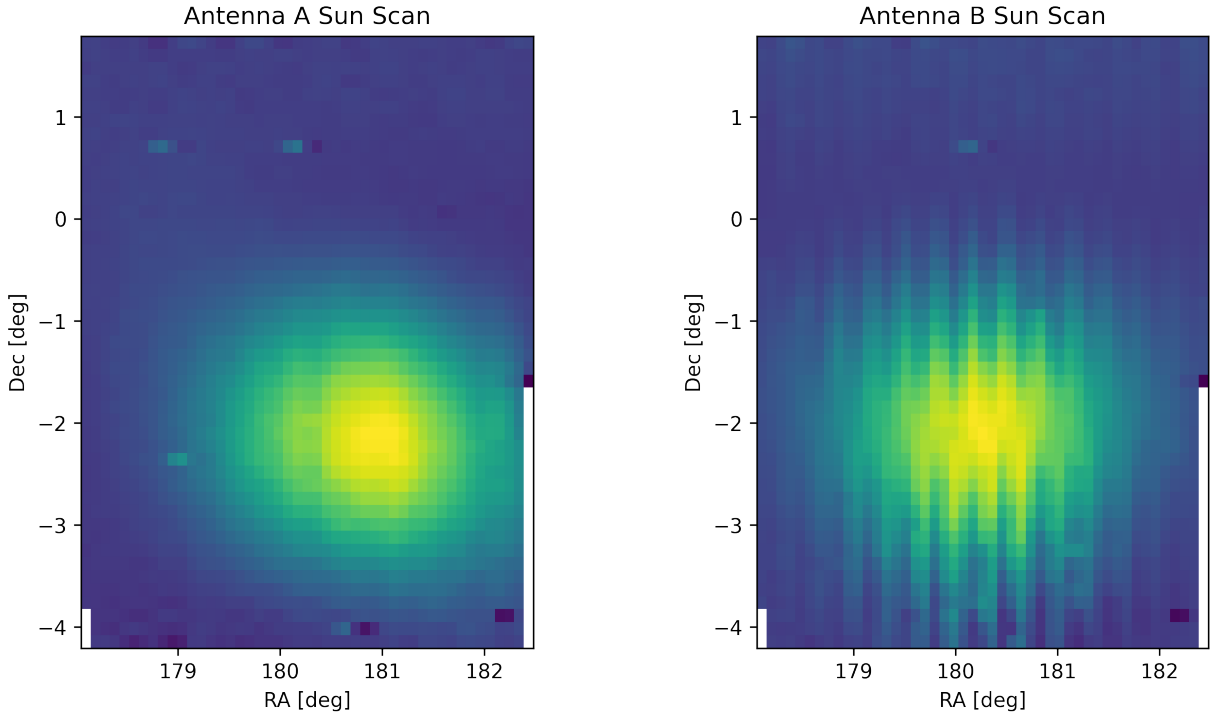

(a) Image from the first antenna

(b) Image from the second antenna

Figure 32: Image of the sun from the antennas

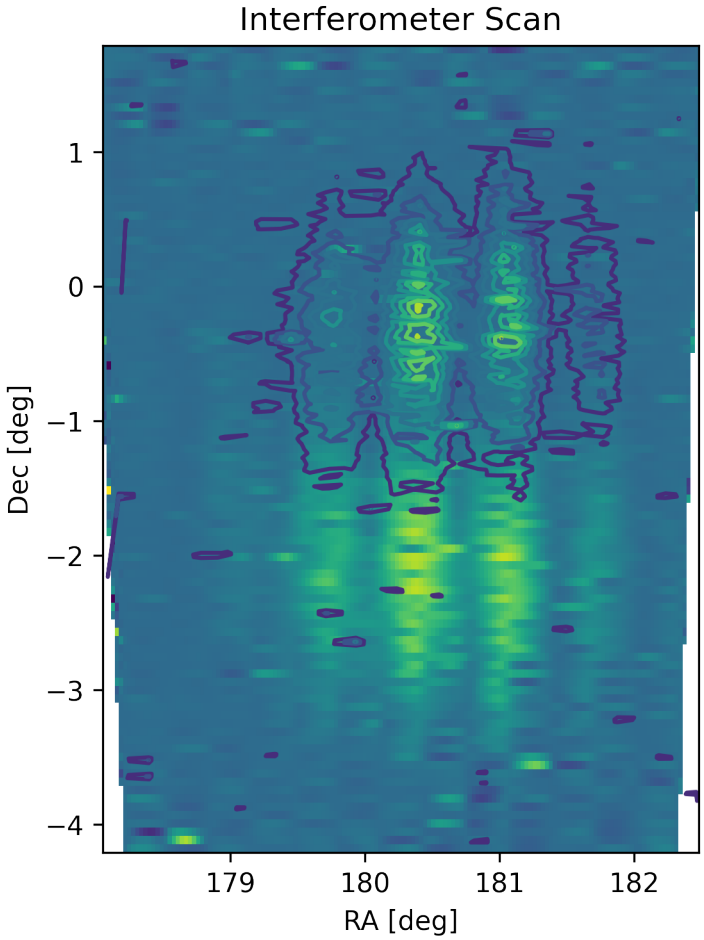

Figure 33: Interferometric image of the Sun

3.2.4 Determination of Diameter of Sun

We can now calculate the diameter of the sun from our interferometric data using:

$$Diameter = \theta \times Distance \tag{11}$$

where θ is the angular diameter, obtained from the is $1^\circ = 0.0174533 radians$. Using the distance between the Earth and the Sun, the diameter of the sun is then calculated to be $2.6 \times 10^6 km$.

4 Conclusion

In the first part of the setup characteristics of various components of the superheterodyne receiver were analysed. We specially focused on three amplifiers, a mixer and two filters. For the three amplifiers, it was observed to work in the linear regime and the gain of the amplifiers was found out. For filters, the plateau-like bandpass spectrum was observed and various parameters of the filter were calculated. Mixer was also observed to work in the linear regime and the conversion loss for it was found to be in typical range for the device. The next step was to calibrate the receiver. This was done using hot-cold calibration of a resistor. The calibration factors were derived and subsequently receiver temperature of the noise diode was also calculated. To estimate how the superheterodyne receiver would work for radio signals attenuated by the earth's atmosphere, an attenuator was also attached to the receiver and power for different attenuators was measured. The output power/receiver temperature shad an exponential decrease with the increase in attenuation as expected from the radiative transport equation. Then the radio spectrum of the signals were analysed for different integration time. The receiver temperature showed a slight increase i.e. SNR increase with an increase in integration time, as expected from the radiometer equation. The line flux and brightness temperature were also each of the radio spectrum. Thus, we see the superheterodyne setup is capable of measuring the radio signals in a desired frequency range depending on the astrophysical source.

The second part of the experiment involved setting up a twin radio interferometer. First, the properties of the telescope and solar radio emission were theoretically studied. The process of collection of data involved setting up the two dishes and operating the interferometer. A still scan and a declination scan were performed. Raw data was obtained and analysed and then removed of noise to obtain the denoised data. This was then used to create an image of the sun from the two antennas and an interferometric image, which was subsequently used to approximate the diameter of the sun.

References

[1] *Radio Astronomy Lab*. English. TheArgelander-InstitutfürAstronomie(AIfA).

[2] U. Klein. *Radio astronomy: tools, applications and impacts*. Argelander-Institut fur Astronomie Bonn. jan 2006. URL: https://astro.uni-bonn.de/~uklein/teaching/radio/files/Radioastronomy.pdf.

[3] Robert Sobot. *Wireless Communication Electronics*. Springer US, 2012. DOI: 10.1007/978-1-4614-1117-8. URL: https://doi.org/10.1007/978-1-4614-1117-8.

[4] *EMC Analysis: Calculate Filter Insertion Loss*. 2023. EMI Software LLC. 2017. URL: https://www.emisoftware.com/blogs/emc-analysis-calculate-filter-insertion-loss/.

[5] *Adjacent Channel Selectivity*. URL: https://www.electronics-notes.com/articles/radio/radio-receiver-selectivity/adjacent-channel-selectivity.php.

[6] *Principles and Applications of RF/Microwave in Healthcare and Biosensing*. Elsevier, 2017. DOI: 10.1016/c2014-0-03378-3. URL: https://doi.org/10.1016/c2014-0-03378-3.

[7] *Mixer Conversion Loss*. PDF document. Institute of Information Science, university of kansas. URL: https://www.ittc.ku.edu/~jstiles/622/handouts/Mixer%20Conversion%20Loss.pdf.

[8] Ericnbsp; O. LEBIGOT. *Welcome to the uncertainties package¶*. URL: https://pythonhosted.org/uncertainties/.

[9] *FM Dipole Antenna*. Accessed on 2023-10-12. URL: https://www.elprocus.com/dipole-antenna/#:~:text=FM%20Dipole%20Antenna&text=This%20is%20a%20half%2Dwave,88%20MHz%20%E2%80%93%20to%20108%20MHZ.

[10] Alexander I. Shapiro, Hardi Peter, and Sami K. Solanki. "The Sun's Atmosphere". In: *Unknown Journal* (2019). Corresponding: someofus@mps.mpg.de. URL: https://www2.mps.mpg.de/projects/solve/files/Solar_Atmosphere.pdf.

[11] Wikipedia Contributors. *Chromosphere*. [Online; accessed 25-September-2023]. 2023. URL: https://en.wikipedia.org/wiki/Chromosphere.

[12] Wikipedia Contributors. *Solar Radio Emission*. [Online; accessed 25-September-2023]. 2023. URL: https://en.wikipedia.org/wiki/Solar_radio_emission.

[13] Wikipedia Contributors. *Planck's Law*. [Online; accessed DD-Month-YYYY]. 2023. URL: https://en.wikipedia.org/wiki/Planck%27s_law.

[14] *Solar Activity Cycle*. Accessed: September 25, 2023. URL: https://pages.uoregon.edu/imamura/122/lecture-6/solar_activity_cycle.html.

[15] Christian Ho et al. "Solar Brightness Temperature and Corresponding Antenna Noise Temperature at Microwave Frequencies". In: *IPN Progress Report* 42 (2008), p. 175.

[16] NASA National Solar Observatory. *Layers of the Sun*. Accessed: September 25, 2023. 2012. URL: https://www.nasa.gov/image-article/layers-of-sun/.

[17] Wikipedia Contributors. *X Band*. https://en.wikipedia.org/wiki/X_band. [Online; accessed 25-September-2023]. 2023.